

# Exoplanet phase curves: observations and theory

Vivien Parmentier and Ian J. M. Crossfield

**Abstract** Phase curves are the best technique to probe the three dimensional structure of exoplanets' atmospheres. In this chapter we first review current exoplanets phase curve observations and the particular challenges they face. We then describe the different physical mechanisms shaping the atmospheric phase curves of highly irradiated tidally locked exoplanets. Finally, we discuss the potential for future missions to further advance our understanding of these new worlds.

## Observing exoplanetary phase curves

### *Origin and shape of a phase curve*

Planetary atmospheres are intrinsically three-dimensional objects, with both small- and large-scale variations of temperature, chemistry, and cloud coverage. This is even more important for the current population of characterizable exo-atmospheres, as most of them belong to planets in close-in orbits, probably tidally locked, with a large day/night temperature contrast induced by permanent radiative forcing. When ignored, the large spatial inhomogeneities of these planets can lead to a biased interpretation of transiting and secondary eclipse observations (Line and Parmentier 2016; Feng et al. 2016).

Observing the phase curve of an exoplanet (i.e., the time-dependent change in the brightness of a planet as seen from Earth during one orbital period) is the most

---

Vivien Parmentier

University of Arizona, Lunar and Planetary Laboratory, 1629 E University Blvd, Tucson, AZ, USAe-mail: vivien@lpl.arizona.edu

Ian J. M. Crossfield

Department of Physics, Massachusetts Institute of Technology, Cambridge, MA, USA e-mail: iancross@mit.edu

straightforward way to probe the planet's longitudinal structure. The brightness of the planet is determined by the combined emitted and reflected light in the particular bandpass of the observations. For transiting planets, the shape and amplitude of the phase curve are determined by longitudinal inhomogeneities. Inhomogeneous illumination is always present, as over the course of one orbit, we see different hemispheres of the planet, ranging from its dayside (before and after the eclipse of the planet by the star) to its nightside. Inhomogeneities in temperatures can be probed by the thermal emission of the planet, with a nightside that is usually colder and thus dimmer than the dayside. Finally, inhomogeneous chemical composition and cloud coverage can be determined through the phase curve's wavelength dependence and shape.

Short-period planets are good targets for atmospheric characterization through phase curve observations: their short orbit makes it easier to monitor the system during a full orbit of the planet. Moreover, planets in orbits  $\lesssim 10$  days are likely tidally locked (Guillot et al. 1996; Parmentier et al. 2015), meaning that their rotation period is their orbital period and that the longitude of the Earth-facing hemisphere can be related to the phase of the orbit. Finally, tidally locked planets in short orbit have a short radiative timescale, a weak Coriolis force, and an input of energy at large scale, making them likely to have planetary-scale atmospheric features that can be observed in the hemispherically averaged planetary flux (Showman and Guillot 2002).

### ***From phase curves to atmospheric properties***

For a steady-state atmosphere, a phase curve provides the longitudinal variation of the hemispherically averaged brightness of the planet. As such, only large-scale atmospheric structures can be inferred (see chapter by Cowan and Fuji). From current phase curve observations, three parameters can usually be retrieved (e.g. Cowan and Agol 2008; Demory et al. 2013; Knutson et al. 2009, 2012). For transiting planets, these parameters are the secondary eclipse depth, the phase of the maximum of the phase curve compared to the secondary eclipse (called the phase curve offset), and the phase curve relative amplitude,  $A_F = (F_{p,\text{Max}} - F_{p,\text{Min}})/F_{p,\text{Max}}$  (see Fig. 1).

The secondary eclipse depth gives the brightness of the dayside hemisphere (see chapter by Roi Alonso) and serves as a reference to calculate  $A_F$ .

The phase offset gives the longitude of the brightest hemisphere of the planet. A planet with a maximum brightness at the substellar point and a symmetrical brightness distribution will have a phase curve peaking during the secondary eclipse. A planet that is brighter *east* of the substellar point will have a phase curve peaking *before* secondary eclipse, leading, by definition, to a *positive* offset of the phase curve maximum. A planet that is brighter *west* of the substellar point will have a phase curve peaking *after* secondary eclipse, leading to a *negative* offset. Here we define *east* and *west* with respect to the rotation of the planet. For tidally locked planets,

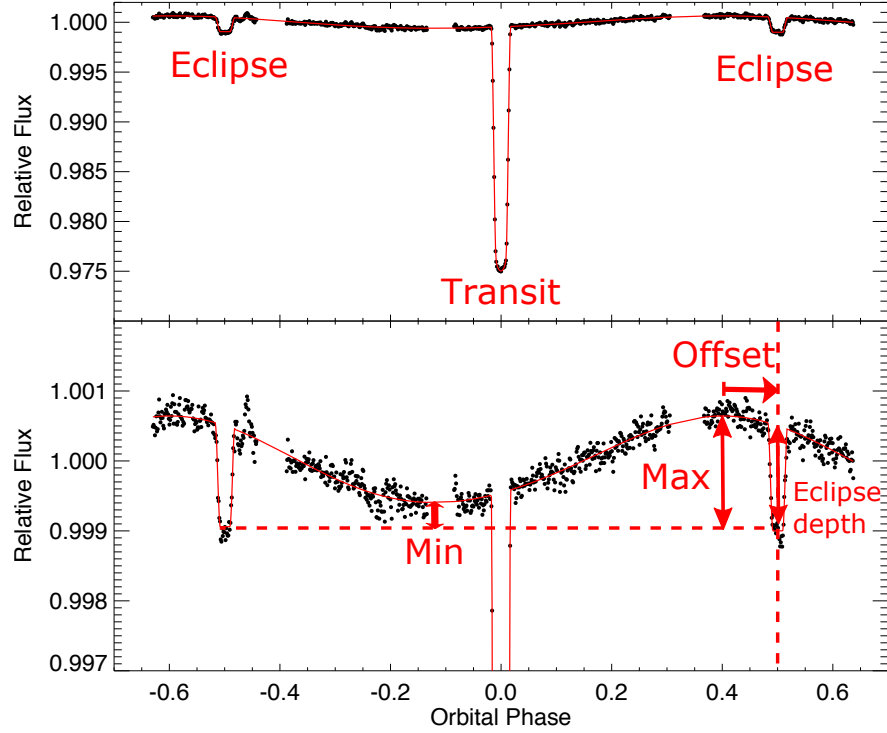


**Fig. 1** Phase curve of HD189733b observed at  $3.6\mu\text{m}$  with the Spitzer Space Telescope by Knutson et al. (2012). The bottom panel is a zoomed-in version of the top panel, with the quantities of interest annotated.

the rotation and the revolution have the same direction and the link between phase curve offset and brightness distribution is independent of the observer’s position.

The phase curve relative amplitude  $A_F$  provides insight into the brightness contrast between the brightest and the dimmest hemisphere. It goes from 0 (corresponding to no brightness variation) to 1 (when one hemisphere emits zero flux). Different flavors of this parameter can be used. As an example, Perez-Becker and Showman (2013) defined the day/night relative amplitude  $(F_{\text{p,Day}} - F_{\text{p,Night}})/F_{\text{p,Day}}$ , whereas Komacek and Showman (2016) used the day/night brightness temperature contrast. The day/night contrast is useful when studying the energy balance of the atmosphere (Cowan et al. 2012; Schwartz and Cowan 2015), but its estimated value can depend on the measurement of the phase curve offset (Schwartz et al. 2017). The temperature contrast might seem a more intuitive quantity, however, for phase curves sparsely sampling the spectral space, the conversion from flux to temperatures is model dependent (Cowan et al. 2012).

For massive planets, gravitational interactions between the planet and the star can lead to non-atmospheric signals in the phase curve such as the ellipsoidal variations and the beaming effect (Shporer 2017). Although techniques can be used to

isolate the atmospheric component of the phase curve, it inevitably leads to higher uncertainties in the derived atmospheric properties ([Shporer and Hu 2015](#)).

## ***Observational Challenges***

Phase curves are a uniquely challenging phenomenon to observe. The timescale and characteristic shape of phase curves make them much more difficult to observe than occultations. While the magnitude of a phase curve signal is comparable to that of the more commonly observed transits or eclipse, the phase curve timescale  $\sim$ days is much longer than the  $\sim$ hour timescale of occultations. Furthermore, phase curves contain only low-frequency components ([Cowan and Agol 2008](#)), while the high-frequency component is much more prominent in transits and eclipses. Occultation observations can be safely decorrelated even against high-order polynomials or complicated and/or periodic signals (e.g., [Haynes et al. 2015](#)), which is much more challenging for phase curves.

In contrast, a single phase curve observation can be compromised by just a single monotonic trend. For example, it took five years to recognize that  $\sim$ 40% of the originally published Spitzer/IRAC  $8\text{ }\mu\text{m}$  phase curve of HD 189733b was compromised by systematics ([Knutson et al. 2007, 2012](#)). Similarly, the Spitzer/MIPS  $24\text{ }\mu\text{m}$  phase curve of HD 209458b was irretrievably compromised by an instrumental drift lasting tens of hours ([Crossfield et al. 2012](#)). In such analyses, as with the case of the apparent ellipsoidal variation seen around WASP-12b at  $4.5\text{ }\mu\text{m}$  ([Cowan et al. 2012; Stevenson et al. 2014a](#)), the question is often: how does one distinguish signal from systematic?

The most straightforward solution is probably also the most effective: repeat the experiment, and observe multiple phase curves at the same wavelengths. This is the approach adopted in the first HST/WFC3 1.1–1.7  $\mu\text{m}$  *spectroscopic* phase curve, of WASP-43b ([Stevenson et al. 2014b](#)). By observing three phase curves, a simultaneous analysis allowed the phase curve to be fit while separating out a long quadratic systematic in addition to the standard HST effects. While multiple observations with the same instrument do not guarantee repeatability ([Stevenson et al. 2017](#)), this approach at least ensures that questionable results are identified. Beyond observing multiple phase curves, a more fundamental requirement is to at least observe a full phase curve – i.e., begin and end with a secondary eclipse – whenever possible.

Implicit in the above comments is the assumption of a continuously observed phase curve. The first phase curve observations employed a more parsimonious, “snapshot” approach using as few as five discrete-observing epochs ([Harrington et al. 2006](#)). This analysis was followed by a combined, snapshot plus continuous, program that measured a mid-infrared phase curve and confirmed the long-term stability of the MIPS  $24\text{ }\mu\text{m}$  detector in most cases ([Crossfield et al. 2010](#)). Later, with the benefit of over a decade of Spitzer analyses, [Krick et al. \(2016\)](#) demonstrated the ability of Spitzer/IRAC to also obtain snapshot-mode phase curves. Caution may be advised since the phase curve amplitudes derived from the IRAC snapshot and from

continuous observations (Wong et al. 2015) differ by  $\sim 5\sigma$ . However, the snapshot technique is not obviously flawed – even multiple continuous phase curves of the same target sometimes disagree by up to  $\sim 4\sigma$  (Stevenson et al. 2017). Regardless, the snapshot technique is unlikely to dominate in the JWST era owing to the large overheads associated with even modest telescope slews.

### ***Wavelength dependence***

Observing exoplanet phase curves at different wavelengths is essential to obtain a complete view of their atmosphere. At optical wavelengths, where the brightness of the planet is often dominated by reflected light, the phase curve provides information on the longitudinal variation of the planet’s albedo. At infrared wavelengths, where the brightness of the planet is often dominated by thermal emission, the phase curve provides information on the longitudinal variation of the planet’s temperature and chemical composition.

The spectral variation of thermal phase curves is shaped by molecular features. Inside a molecular absorption band, a phase curve probes low pressures (high altitudes) while probing deeper outside a molecular absorption band (Showman et al. 2009; Kataria et al. 2015). As a consequence, multiwavelength phase curves probe 2D (longitude, depth) thermal and chemical structure of the atmosphere (Knutson et al. 2009; Stevenson et al. 2014b, 2017). In general, there is no reason to believe that phase curves obtained in different bandpasses will be similar. When looking for trends between the amplitude or offset of phase curves and planetary parameters, it is therefore important to compare observations taken in the same bandpasses.

In some bandpasses, both reflected light and thermal emission can contribute significantly. Fig. 2 shows the theoretical reflected and thermal phase curves of a hot Jupiter in the Kepler bandpass (400–800nm). The reflected phase curve is dominated by the presence of bright clouds west of the substellar point, whereas the thermal emission phase curve is dominated by the presence of a temperature maximum east of the substellar point. For this specific model ( $T_{\text{eq}} = 1900\text{K}$ ) and bandpass, thermal emission and reflected light compensate, and no offset is measured. For cooler planets, reflected light should dominate over thermal emission, whereas for hotter planets it should be the opposite, leading to the correlation between phase curve offset and equilibrium temperature for Kepler phase curves seen in the right panel of Fig. 2.

### ***Summary of observations to date***

Table 1 lists the current phase curve observations of transiting exoplanets, while Fig. 3 shows the observations for the thermal phase curves of hot Jupiters. In general, hot Jupiters’ thermal phase curves have a large amplitude (between 0.5 and 1)

**Table 1** Current exoplanets phase curve observations

| Planet                   | $T_{\text{eq}}^e (K)$ | P (days) | $\lambda (\mu\text{m})$ | $A_F$             | Offset ( $^\circ$ ) | Reference  |
|--------------------------|-----------------------|----------|-------------------------|-------------------|---------------------|--|
| 55 CnC e                 | 1958                  | 0.74     | 4.5                     | $0.76 \pm 0.27$   | $41 \pm 12$         | <a href="#">Demory et al. (2016)</a>             |
| GJ436b <sup>g</sup>      | 770                   | 2.64     | 8                       | $0.40 \pm 0.13$   | $4 \pm 26$          | <a href="#">Stevenson et al. (2012)</a>          |
| HAT-P-7b                 | 2226                  | 2.2      | 0.6                     | $1.02 \pm 0.04^c$ | $7.9 \pm 0.3^a$     | <a href="#">Esteves et al. (2015)</a>            |
|                          |                       |          | 3.6                     | $0.8 \pm 0.15$    | $6.8 \pm 7.5$       | <a href="#">Wong et al. (2016)</a>               |
|                          |                       |          | 4.5                     | $0.6 \pm 0.11$    | $4.1 \pm 7.5$       | <a href="#">Wong et al. (2016)</a>               |
| HD149026b                | 1645                  | 2.87     | 8                       | $0.70 \pm 0.34$   | n/a                 | <a href="#">Knutson et al. (2009)</a>            |
| HD189733b                | 1198                  | 2.218    | 3.6                     | $0.845 \pm 0.061$ | $35.8 \pm 4$        | <a href="#">Knutson et al. (2012)</a>            |
|                          |                       |          | 4.5                     | $0.55 \pm 0.06$   | $20.1 \pm 5.5$      | <a href="#">Knutson et al. (2012)</a>            |
|                          |                       |          | 8                       | $> 0.096$         | $23.7 \pm 2.7$      | <a href="#">Knutson et al. (2012)</a>            |
|                          |                       |          | 24                      | $0.26 \pm 0.08$   | $37.2 \pm 8.1$      | <a href="#">Knutson et al. (2012)</a>            |
| HD209458b                | 1445                  | 3.52     | 4.5                     | $0.71 \pm 0.05$   | $40.9 \pm 6$        | <a href="#">Zellem et al. (2014)</a>             |
| $\nu$ And b <sup>f</sup> | 1233                  | 4.62     | 24                      | n/a               | $84.5 \pm 6.3$      | <a href="#">Crossfield et al. (2010)</a>         |
| WASP-12b                 | 2990                  | 1.09     | 3.6                     | $0.90 \pm 0.19^b$ | $53 \pm 7^d$        | <a href="#">Cowan et al. (2012)</a>              |
|                          |                       |          | 4.5                     | $0.95 \pm 0.12^b$ | $16 \pm 4$          | <a href="#">Cowan et al. (2012)</a>              |
| WASP-14b                 | 1875                  | 2.24     | 3.6                     | $> 0.91$          | $9.56 \pm 1.4$      | <a href="#">Wong et al. (2015)</a>               |
|                          |                       |          | 4.5                     | $0.70 \pm 0.06$   | $6.75 \pm 1.4$      | <a href="#">Wong et al. (2015)</a>               |
| WASP-18b                 | 2396                  | 0.94     | 1.5                     | $> 0.93$          | $7 \pm 2$           | <a href="#">Arcangeli et al. (2017)</a>          |
|                          |                       |          | 3.6                     | $0.97 \pm 0.09$   | $0.3 \pm 1$         | <a href="#">Maxted et al. (2013)<sup>b</sup></a> |
|                          |                       |          | 4.5                     | $0.96 \pm 0.06$   | $-3.6 \pm 2.3$      | <a href="#">Maxted et al. (2013)<sup>b</sup></a> |
| WASP-19b                 | 2064                  | 0.79     | 3.6                     | $0.96 \pm 0.11$   | $10.45 \pm 4$       | <a href="#">Wong et al. (2016)</a>               |
|                          |                       |          | 4.5                     | $0.81 \pm 0.12$   | $12.9 \pm 3.6$      | <a href="#">Wong et al. (2016)</a>               |
| WASP-43b                 | 1441                  | 0.81     | 1.5                     | $1.005 \pm 0.013$ | $12.3 \pm 1.0$      | <a href="#">Stevenson et al. (2014b)</a>         |
|                          |                       |          | 3.6                     | $1 \pm 0.03$      | $12.2 \pm 1.7$      | <a href="#">Stevenson et al. (2017)</a>          |
|                          |                       |          | 4.5                     | $1 \pm 0.03$      | $21 \pm 1.8$        | <a href="#">Stevenson et al. (2017)</a>          |
| WASP-103b                | 2508                  | 0.92     | 1.5                     | $0.93 \pm 0.055$  | $-3.7 \pm 3.8$      | <a href="#">Kreidberg et al. (2017)</a>          |
|                          |                       |          | 3.6                     | n/a               | n/a                 | <a href="#">Kreidberg et al. (2017)</a>          |
|                          |                       |          | 4.5                     | $0.82 \pm 0.055$  | $6.3 \pm 2.6$       | <a href="#">Kreidberg et al. (2017)</a>          |
| Kepler-7b                | 1630                  | 4.88     | 0.6                     | $1.12 \pm 0.38^c$ | $-25 \pm 1.9$       | <a href="#">Esteves et al. (2015)</a>            |
| Kepler-8b                | 1680                  | 3.52     | 0.6                     | $0.74 \pm 0.45^c$ | $-24.8 \pm 5.6$     | <a href="#">Esteves et al. (2015)</a>            |
| Kepler-10b               | 2120                  | 0.83     | 0.6                     | $1.12 \pm 0.27$   | $9 \pm 6$           | <a href="#">Hu et al. (2015)</a>                 |
| Kepler-12b               | 1480                  | 4.43     | 0.6                     | $0.89 \pm 0.26^c$ | $-44.3 \pm 5.8$     | <a href="#">Esteves et al. (2015)</a>            |
| Kepler-41b               | 1770                  | 1.86     | 0.6                     | $1.30 \pm 0.48^c$ | $-31 \pm 5$         | <a href="#">Esteves et al. (2015)</a>            |
| Kepler-76b               | 2140                  | 1.54     | 0.6                     | $0.80 \pm 0.05^c$ | $8.3 \pm 1.2$       | <a href="#">Esteves et al. (2015)</a>            |

For optical phase curves, only planets for which an offset is detected have been considered. The phase curves of highly eccentric planets are discussed in a later section.

Only planets on circular orbits have been taken into account here, a discussion of eccentric planets can be found in the devoted section.

Instruments used are Spitzer for the 3.6, 4.5, 8 and 24 $\mu\text{m}$  observations, HST/WFC3-IR for the 1.5 $\mu\text{m}$  observations, Kepler for the 0.6 $\mu\text{m}$  observations

<sup>a</sup> The offset varies from orbit to orbit ([Armstrong et al. 2016](#)) <sup>b</sup>  $A_F$  values were taken from [Stevenson et al. \(2017\)](#) <sup>c</sup> Uncertainty for phase curve maximum observed in the Kepler bandpass was assumed to be similar to the uncertainty of the secondary eclipse. <sup>d</sup> Using a different noise model the same authors get an offset of  $0 \pm 29$ .

<sup>e</sup> We use  $T_{\text{eq}}^4 = \frac{T_{\text{star}}^4 R_{\text{star}}^2}{4a^2}$ ,  $a$  : semi-major axis,  $T_{\text{star}}$ ,  $R_{\text{star}}$  : stellar effective temperature and radius. <sup>f</sup> This is a non transiting planet with a measured inclination of  $24 \pm 4^\circ$  ([Piskorz et al. 2017](#)). <sup>g</sup> This planet has a non-zero but small eccentricity ( $e=0.1371$ ) (see [Stevenson et al. 2010](#)).

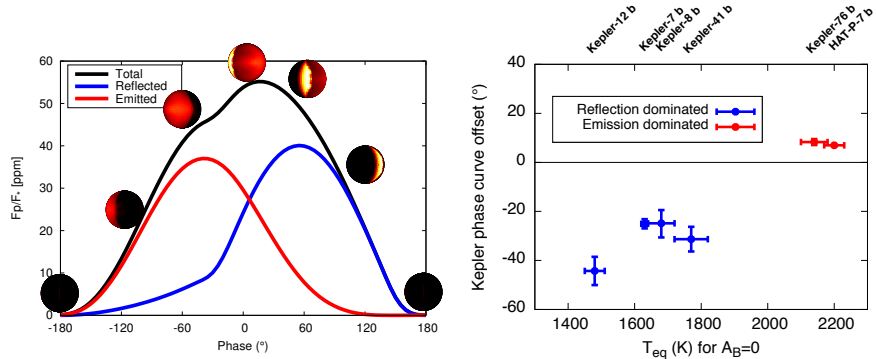


**Fig. 2** *Left* : Phase curve in the Kepler bandpass calculated from a hot Jupiter model with  $T_{eq} = 1900\text{K}$  including silicate clouds. The phase curve (black) is a combination of the reflected phase curve (blue) and the thermal emission phase curve (red). The circles are brightness maps of the Earth-facing hemisphere. The bright strip on the east of the substellar point is reflected light due to clouds whereas the rest is thermal emission. *Right* : Observed offsets in the Kepler phase curve sample. Planets with a small equilibrium temperature, dominated by reflected light, have a negative offset, whereas planets with a high equilibrium temperature, dominated by thermal emission, have a positive offset. Figure from [Parmentier et al. \(2016\)](#).

and have a positive offset, meaning that the brightest hemisphere is eastward of the substellar point.

As seen in Fig. 3, there is no clear trend between the amplitude of thermal phase curves and planet equilibrium temperature. Earlier claims by [Perez-Becker and Showman \(2013\)](#) and [Komacek and Showman \(2016\)](#) were based on a smaller number of observations and by interpreting together observations taken in different bandpasses. In today's more complete dataset, no trend is seen, neither by looking at all bandpasses together nor by looking at them separately.

A tentative trend, first proposed by [Stevenson et al. \(2017\)](#), is seen in the amplitude vs. planet rotation period plot: planets with a faster rotation rate might have a larger phase curve amplitude. Observations of planets with an orbital period between 1 and 2 days and, especially, larger than 3 days are currently being taken to confirm the presence of a correlation (Spitzer program 13038).

The most striking feature of Fig. 3 might be in the phase curve offset vs. equilibrium temperature plot, with a lack of large offset for planets with equilibrium temperatures  $\gtrsim 1700\text{ K}$ . WASP-12b seems an outlier, but its large offset might be the result of uncorrected instrument systematics ([Cowan et al. 2012](#)). The super-Earth 55 Cnc e does not fit in this trend defined by hot Jupiter observations. Its phase curve appears similar to cooler hot Jupiters, such as HD209458b, which has a large offset and a large phase curve amplitude at  $4.5\mu\text{m}$ , pointing toward unique atmospheric or ground properties.

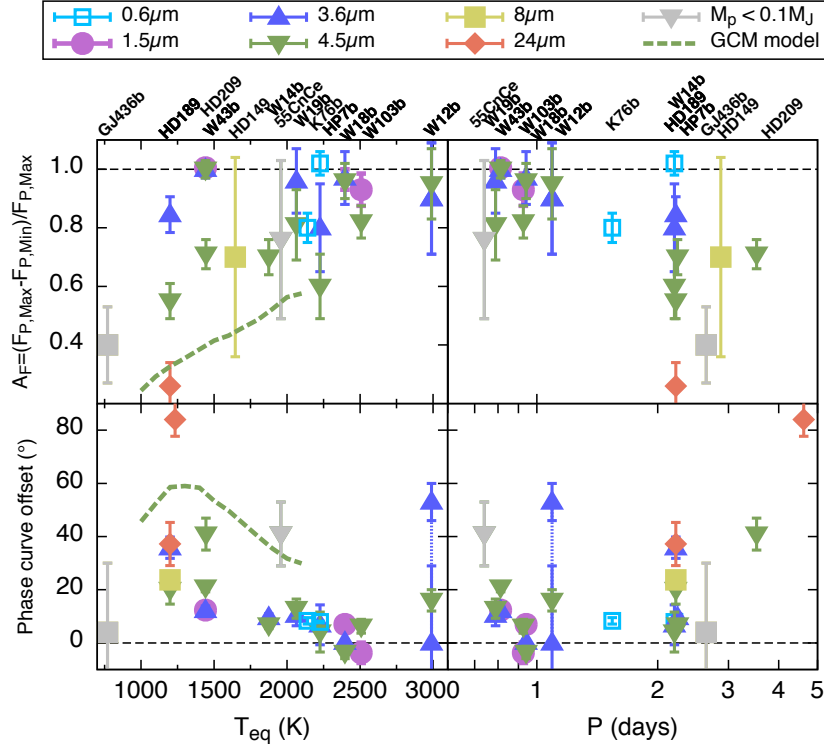


**Fig. 3** Amplitude (top) and offset (bottom) of exoplanet thermal phase curves as a function of equilibrium temperature (left) and orbital period (right). Different symbols and colors represent different wavelengths. Values predicted at  $4.5\mu\text{m}$  by the Jupiter radius, solar composition, chemical equilibrium, cloudless and drag-free global circulation model of Parmentier et al. (2016) are overplotted. The model systematically underpredicts the amplitude and overpredicts the offset of the phase curve. For the  $0.6\mu\text{m}$  case, only planets with a phase curve dominated by thermal emission are considered (i.e. planets with  $T_{\text{eq}} > 2000\text{K}$ ). For WASP-12b, the two possible offsets derived from the same phase curve are linked with a dashed curve (Cowan et al. 2012). Colored points are hot Jupiters, gray points are super-Earths and mini-Neptunes. The data is from Table 1.

## The physics of exoplanet phase curves

### Thermal structure

#### Atmospheric regimes

In response to the large day-to-night irradiation gradient, tidally locked planets develop a strong atmospheric circulation that advects energy from the dayside to the nightside and reduces the day/night temperature contrast compared to the local radiative equilibrium case. However, energy losses by radiation or by the damping of

the winds can prevent a fully efficient redistribution of energy. This balance between energy transport and energy losses can be understood in terms of timescales (Showman and Guillot 2002; Komacek and Showman 2016). The radiative timescale is the characteristic time it takes for a parcel of gas to lose its energy by radiation. The wave timescale is the time it takes for a gravity wave to travel horizontally over one planetary radius. The drag timescale is the time it takes for the waves or the winds to lose a significant part of their kinetic energy.

Depending on the balance between these three timescales, the atmospheric circulation on tidally locked planets is expected to follow at least two different regimes (see also chapter by N. Lewis). When the radiative timescale and the drag timescales are similar or longer than the wave timescale, the presence of an eastward, equatorial jet is expected. The resulting temperature map is shifted eastward compared to a local radiative equilibrium case, and the hottest spot of the atmosphere lays eastward of the substellar point. When the radiative timescale or the drag timescale is smaller than the wave timescale, the atmospheric circulation is characterized by a day-to-night flow with a temperature map symmetric around the substellar point and a somewhat larger hemispheric temperature contrast (e.g. Showman and Polvani 2011; Tsai et al. 2014).

### Phenomenological models vs. global circulation models

The energy balance of a planet can be determined by measuring the thermal emission from two opposite hemispheres. When considering the day- and nightside hemispheres, one can understand the energy balance in terms of how much of the incoming energy is reflected to space (i.e., the Bond albedo) and how much of the absorbed stellar light is transferred to the nightside (i.e., the redistribution factor). In order to have a complete energy balance, the full dayside and nightside spectra should be used. However, current observations only cover a few bandpasses, and the effective temperature of each hemisphere must be estimated by extrapolating the measurements with assumptions that are only exact if each hemisphere emits like a blackbody. These approximations should work for the planet's dayside (Cowan and Agol 2011a) but might fail when estimating the nightside temperatures (Schwartz and Cowan 2015) where the vertical temperature gradient is larger. The latest results from Schwartz et al. (2017) show a large dispersion in both redistribution efficiency and geometric albedo between planets, with no apparent trend between equilibrium temperature and day/night temperature contrast, echoing the lack of trends seen in the top left panel of Fig. 3. Schwartz et al. (2017) also conclude that many hot Jupiters have Bond albedos larger than 0.3, in apparent contradiction with their measured low geometric albedos in the Kepler bandpass (Heng and Demory 2013). This apparent discrepancy could be the result of an asymmetric scattering function (e.g., Dyudina et al. 2005), a lower geometric albedo in the Kepler bandpass than outside of it (Crossfield 2015), or an intrinsic bias in the method.

Linking the phase curve amplitude and the phase offset is a more complex task that requires a model of the longitudinal distribution of the temperature and the

opacities. One (and two) -dimensional models of the longitudinal (and latitudinal) variation of the temperature have been calculated by taking into account the competing effects of longitudinal advection of energy and radiative losses (Cowan and Agol 2011b; Hu et al. 2015; Zhang and Showman 2017). They lead to a temperature map that is determined by one parameter: the ratio of the advective and the radiative timescale. Consequently, they always predict a correlation between the phase curve offset and the phase curve amplitude. These models, however, lack vertical transport, which is proven to be an important factor setting the day/night temperature contrast (Komacek and Showman 2016). The phase curve offset and the phase curve amplitude might therefore be set by different mechanisms, which could be the reason why they are not correlated in the observations (Crossfield 2015) nor in the more complex, three-dimensional models of tidally locked exoplanets (Komacek et al. 2017; Parmentier et al. 2016).

Whereas these phenomenological models are useful to retrieve parameters such as the radiative timescale from phase curve observations, they can't say much about the mechanisms setting these parameters. Global circulation models, solving for the hydrodynamics, the radiative transfer, and/or the magnetic effects in three dimensions, have been used to quantitatively link the observed day/night contrast and phase curve offset to planetary parameters. As seen in Fig. 3, cloudless, dragless, solar composition models systematically underpredict the amplitude and overpredict the offset of thermal phase curves (Showman et al. 2009; Kataria et al. 2015). Other mechanisms, such as metallicity (Kataria et al. 2015), cloud composition (Oreshenko et al. 2016; Parmentier et al. 2016), rotation period (Showman et al. 2009; Showman and Polvani 2011), disequilibrium chemistry (Cooper and Showman 2006), or magnetic field strength (Rogers 2017) must play an important role.

### Radiative timescale

The radiative timescale is expected to vary linearly with pressure and with the inverse of the cube of the temperature (Iro et al. 2005; Showman et al. 2008). Since the pressures probed by atmospheric sensing span several orders of magnitude, the pressure dependence of the radiative timescale has a major consequence on the observations. Phase curves obtained at wavelengths probing deep in the atmosphere are expected to probe layers with a large radiative timescale and thus a small amplitude and a large offset, whereas phase curves obtained at wavelengths probing shallower layers (e.g., inside molecular bands) should have a larger amplitude and smaller offset. This is illustrated in the cloudless case of Fig. 6.

The temperature dependence of the radiative timescale is also expected to impact the observations. With all things being equal, hotter planets are expected to cool more efficiently, leading to a larger day/night temperature contrast and thus a larger phase curve amplitude (Perez-Becker and Showman 2013; Komacek and Showman 2016). As seen in Fig. 3, the lack of a clear trend in the amplitude vs. equilibrium

temperature plot indicates that other mechanisms must contribute to the shape of exoplanets' phase curves (Komacek et al. 2017).

### Drag, composition and mean molecular weight

The thermal structure of the planet can be affected when either the radiative timescale, the drag timescale, or the wave timescales are changed.

Atmospheric drag is often used and parametrized as Rayleigh drag in models to represent different types of physical mechanisms such as shocks (Perna et al. 2012; Heng 2012), hydrodynamic instabilities (Fromang et al. 2016) or Lorentz forces (Perna et al. 2010; Batygin et al. 2013). Its main effect is to weaken the super-rotating jet, leading to a more pronounced substellar to anti-stellar flow and a weaker equatorial eastward jet. As seen in Fig. 4, small Rayleigh drag ( $\tau_{\text{drag}} \approx 10^5$  s) has a small effect on the phase curve amplitude but a large effect on the phase offset. By shifting the circulation pattern from a jet-dominated to a day-to-night flow, a small drag does not change much the heat transport to the nightside but reduces the longitudinal asymmetry of the temperature and therefore the phase curve offset. A larger drag (e.g.,  $\tau_{\text{drag}} \approx 10^3 - 10^4$  s) can increase the phase curve amplitude significantly, but lead to an extremely small phase curve offset. It is important to keep in mind that the physical mechanism responsible for the drag might not be homogeneous in the atmosphere or might not even act as a Rayleigh drag at all. For example, Lorenz forces should have a fundamentally different effect on the flow than Rayleigh drag, leading to a potential inversion of the equatorial jet speed (Rogers and Komacek 2014; Rogers 2017), whereas hydrodynamic instabilities and shocks should drag the flow where large velocity or temperature gradients are present (Fromang et al. 2016; Heng 2012).

Atmospheric composition can also play an important role in shaping the phase curve of exoplanets. By increasing the abundance of metals in the atmosphere, metallicity increases the opacities, leading to two consequences. First the atmospheric layers probed are shifted to smaller pressures, where the radiative timescale is smaller leading to a large phase curve amplitude and a smaller phase curve offset. Second the enhanced opacities lead to a warmer atmosphere and thus to a smaller radiative timescale. Overall, increasing the atmospheric metallicity should increase the amplitude and decrease the offset of the phase curve. For WASP-43b, global circulation models with a metallicity of five times solar provide a better, but not satisfactory, match to the observations compared to models assuming a solar metallicity (Kataria et al. 2015).

In planets with equilibrium temperatures larger than  $\approx 1900\text{K}$ , titanium and vanadium oxide are expected to be present in the dayside atmosphere and create a strong thermal inversion (Hubeny et al. 2003; Fortney et al. 2008; Parmentier et al. 2015, 2016). The detection of such an inverted temperature profile has recently been claimed through the presence of molecular emission features in the dayside of both WASP-33b (Haynes et al. 2015) and WASP-121b (Evans et al. 2017). Thermal in-

versions are expected to disappear in the planet's nightside where these molecular features are expected to become absorption features.

In small planets, where the atmospheric composition can be very diverse, the mean molecular weight of the atmosphere is expected to impact both the radiative timescale and the wave timescale. [Zhang and Showman \(2017\)](#) show that the day/night temperature contrast is expected to increase, and the eastward shift of the hot spot is expected to decrease, when the mean molecular weight is increased. In real planets, atmospheres with different mean molecular weight will have a very different composition, leading to variations of several orders of magnitude in the opacities and potentially a comparable or stronger effect than the effect of the mean molecular weight alone.

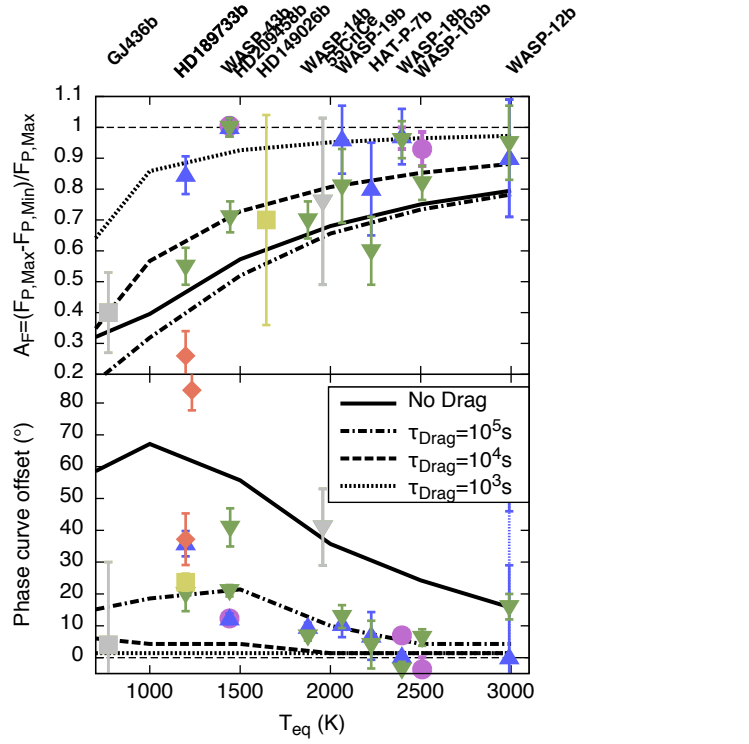


**Fig. 4** Observed thermal phase curve amplitude (upper panel) and offset of the maximum (bottom panel) compared with semi-gray global circulation models from ([Komacek et al. 2017](#)) using different strength of drag. The color and shape of the points are the same as in Fig. 3.

## Opacity structure

### Chemistry

In chemical equilibrium, temperature inhomogeneities often pair up with chemical composition inhomogeneities. For a given atomic composition, equilibrium favors different molecules at different pressures and temperatures. A day/night temperature contrast on a tidally locked planet could result in a day/night chemical gradient. Such a large-scale change in the chemistry should trigger a change in the opacities and affect the offset and the amplitude of the phase curve. Horizontal and vertical advection are expected to further complicate this picture. When the chemical reaction timescale is long compared to the horizontal and the vertical mixing timescale, chemical reactions cannot happen fast enough during the transport of gas from one side to the other side of the planet and quenching happens. The atmospheric circulation can then drive the chemical abundances out of their local equilibrium state and erase any chemical gradient expected from the local equilibrium (Cooper and Showman 2006; Visscher and Moses 2011). The exact chemical composition of the atmosphere is determined by a combination of the chemical equilibrium abundances of the deep atmosphere (vertical quenching) and of the hot dayside (horizontal quenching) (Agúndez et al. 2014). Chemical quenching is expected to affect the opacities in very specific bands, leading to a peculiar signature in the day/night contrast vs. wavelength relationship (Steinrueck et al. 2017).

In very hot planets ( $T_{\text{eq}} \gtrsim 2500\text{K}$ ) molecules such as water should be thermally dissociated at the dayside photosphere but not in the nightside, whereas more strongly bond molecules, such as CO, should be present at all longitudes (see Fig. 5). When molecules dissociate, continuum opacities from hydrogen ions are expected to become dominant, leading to a lack of spectral features and a blackbody-like thermal emission in the dayside (Kreidberg et al. 2017; Arcangeli et al. 2017).

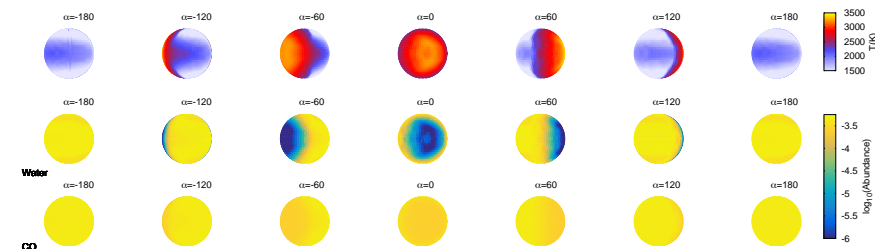


**Fig. 5** Temperature (top) and abundances (water, middle and CO, bottom) at the  $1.4\mu\text{m}$  photosphere of WASP-103b as predicted from global circulation models of Parmentier et al. (2016). The different columns are for different orbital phases,  $\alpha = 0$  being the secondary eclipse. The water abundance drops by two orders of magnitude in the dayside due to thermal dissociation (Kreidberg et al. 2017). The abundances are calculated assuming local chemical equilibrium (Visscher et al. 2006).

## Clouds

The large temperature variations in the atmosphere of tidally locked planets in close-in orbits are responsible for the prevalence of large longitudinal inhomogeneities in their cloud coverage as inferred from the observations (Demory et al. 2013; Shporer and Hu 2015). In each planet, some species can condense in the cold nightside of the planet but must be in gaseous form in the hot dayside (Parmentier et al. 2013). Since the temperature map of most hot Jupiters is not symmetric, but shifted eastward, the western part of the dayside is usually cold and clouds can also form there. The reflected phase curve can then be dominated by the bright reflective part of the dayside atmosphere where clouds are present, leading to a phase curve peaking after secondary eclipse, the opposite sign than for thermal phase curve (see Hu et al. (2015); Garcia Munoz and Isaak (2015); Webber et al. (2015) and Fig 2). The longitudinal distribution of a given type of cloud in the dayside is determined to first order by the thermal structure of the planet and the cloud-specific condensation temperature (Lee et al. 2016). If the thermal structure is known, either by observing a thermal phase curve or by modeling the temperature distribution a priori, the cloud map derived from the reflected light curve can be used to constrain the cloud chemical composition (Oreshenko et al. 2016; Parmentier et al. 2016).

Clouds should also affect the thermal emission of the planet. The presence of nightside clouds produces a large opacity gradient between the day and the night that can suppress the thermal emission from the cloudy regions by raising the photosphere to low pressures. As a consequence, clouds are expected to increase the phase curve amplitude and decrease the phase curve offset of hot Jupiters (see Fig. 6), even if they are present only on the planet’s nightside. When clouds are present, the brightest hemisphere is not necessarily the hottest one, and the shift of the maximum of thermal phase curves does not track the shift of the hottest point of the planet anymore (Parmentier et al. 2017). Similarly, the day/night flux contrast cannot be easily converted to a day/night horizontal temperature contrast, a redistribution parameter or an advective timescale. Any inference of the thermal structure and atmospheric composition of an atmosphere based on the phase offset and the day/night contrast of a thermal phase curve can be highly biased by the presence of clouds. An optical phase curve, probing the planet albedo as a function of longitude seems a necessary complement to any thermal phase curve.

## Time variability

Atmospheres can be time variable, leading to a time dependence of the phase curve amplitude and offset between orbits. Given the large number of observations needed to observe one phase curve and thus the time needed to constrain differences between phase curves, atmospheric variability has not yet been widely characterized. The most notable exception is the planet HAT-P-7b, a hot Jupiter that has been observed continuously by the Kepler spacecraft over more than 700 orbital periods.

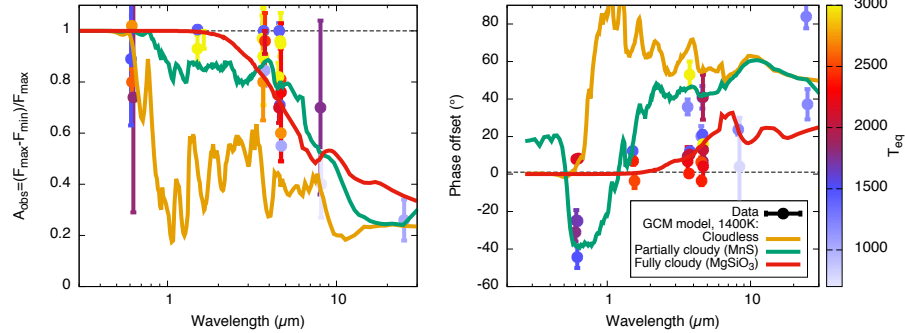


**Fig. 6** Relative amplitude (left) and phase offset (right) of currently known exoplanet phase curves as a function of wavelength. The color of the points represents the equilibrium temperature of the planet. Predictions from three different global circulation models of a hot Jupiter with  $T_{\text{eq}} = 1400\text{K}$  have been overplotted (Parmentier et al. 2017): an example of a cloudless model (orange), a model with a partial cloud coverage (green, assuming the presence of MnS clouds) and an example of a fully cloudy model (red, assuming the presence of  $\text{MgSiO}_3$ ).

As shown by Armstrong et al. (2016), the shift of the maximum of the phase curve may vary from positive to negative values over a timescale of 50 orbits. Two scenarios have been proposed to explain this behavior. In the first scenario, a global change in the dayside temperature of the planet, without necessarily a change in the position of the hot spot, would lead to a variation in the cloud coverage, changing the relative ratio of thermal and reflected contribution to the light curve (Armstrong et al. 2016). In the second scenario, proposed by Rogers (2017), the entire phase curve of HAT-P-7b is dominated by thermal emission. The coupling between the ionized atmosphere and the magnetic field leads to an oscillation in the strength and direction of the equatorial jet and the center of the hottest hemisphere itself oscillates from east to west of the substellar point. Observations of variability at infrared wavelength should be able to disentangle between the two scenarios. In the first case, no variation is expected at infrared wavelengths, where reflected light is never dominant. In the second scenario, the change of the hottest hemisphere longitude should affect similarly the Kepler phase curve and the infrared phase curve.

### Eccentric planets

Highly eccentric planets are laboratories to understand the response of a planet atmosphere to a time-dependent forcing. Quantities that are degenerate in the phase curves of tidally locked planets, such as the radiative timescale and the advective timescale, can potentially be measured separately in the eccentric case (Lewis et al. 2013; de Wit et al. 2016). When passing through periastron, the planet is inhomogeneously and transiently heated. Then, depending of the rotation period of the planet (Hut 1981), the heated hemisphere is expected to face Earth periodically after

periastron, leading observable oscillations (or "ringing") in the phase curve (Langton and Laughlin 2008; Kataria et al. 2013). While the period of these oscillations are related to the rotation period of the planet, their amplitude is linked to the radiative timescale of the atmosphere (Cowan and Agol 2011b). So far, the thermal phase curves of two highly eccentric planets have been published, while the phase curve of a third one (XO-3b) has been observed but is not yet published. No oscillations were found in the thermal phase curves of HAT-P-2b and HD80606b, which was interpreted by the presence of a short ( $\approx 2 - 6$ h) radiative timescale at the photosphere (Lewis et al. 2013; de Wit et al. 2016). Such a short radiative timescale is reproduced by global circulation models of HAT-P-2b (Langton and Laughlin 2008; Lewis et al. 2013) but not by models of HD80606b, where the cooler temperatures predict a longer timescale. Any opacity source, such as clouds, could raise the photosphere of HD80606b to lower pressures and account for this short radiative timescale (Lewis et al. 2017). Planned Hubble Space Telescope observations should measure the albedo of HD80606b and its variation around periastron.

### ***Non-transiting planets***

Phase curve observations can be used to characterize the atmospheres of non-transiting planets on short orbits. The number of non-transiting planets is far greater than the number of transiting ones, so non-transiting planets can potentially provide a large sample of bright planets to study (Millholland and Laughlin 2017). Unfortunately, the phase curve relative amplitude cannot be determined directly for non-transiting, even when the inclination of the system is known, as both the radius of the planet and the stellar absolute flux cannot be measured directly (Crossfield et al. 2010). The phase curve offset, however, can be directly determined from the observation, given a good enough knowledge of the planet ephemeris. So far,  $\nu$  And b is the only non-transiting planet with a known inclination (Piskorz et al. 2017) that has a measured phase curve offset (Crossfield et al. 2010). Measuring a phase curve offset for planets over a wide range of inclinations could be used to infer the latitudinal thermal structure of exoplanets' atmospheres.

### **Future prospects with JWST**

The James Webb Space Telescope (JWST) will provide valuable information on giant tidally locked planets through phase curve observations. By observing both optical infrared wavelengths, NIRISS should be able, in one spectroscopic phase curve observation, to provide both the cloud map and the temperature map of hot Jupiters and show the change of sign of the phase curve offset with wavelength expected for a partially cloudy atmosphere (see Fig. 6). NIRCAM and NIRSPEC will provide valuable measurements of molecular abundances and their variation with

longitude. These near-infrared wavelengths, however, are not best suited to observe the cooler nightside of tidally locked planets where most observations measured a close-to-zero flux and could not detect any molecular features. These cooler nightsides should, however, be brighter at longer wavelengths, where MIRI can observe.

CHEOPS, TESS, and PLATO will significantly increase the number of optical phase curves of hot Jupiters, giving important constraint on the cloud distribution on exoplanets (see [Shporer 2017](#), for a complete review). Moreover, these missions will find numerous planets, particularly in the Neptune size range, that current and future observatories (HST, JWST) will be able to characterize. As such, numerous phase curves of Neptune and sub-Neptune size planets could be obtained during the next decade, increasing drastically the current sample of two (55 CnC e and GJ436b, see Figure 3).

FINESSE and ARIEL, currently into the selection process, would provide hundreds of exoplanets spectroscopic phase curves covering a wide range of planet mass, radius, irradiation and rotation period. Such a survey mission is needed to understand the diversity of climates on extrasolar worlds.

JWST will probably be used to search for the phase curves of temperate rocky planets orbiting M dwarfs ([Kreidberg and Loeb 2016](#)), such as the Trappist-1 planets, Proxima centauri b or LHS 1140b. Theoretically, the phase curve amplitude of these systems can be used to determine whether the planet possesses a fluid that can efficiently transport energy (i.e., an atmosphere or an ocean), since the amplitude of the phase curve of a bare rock would be larger than any other cases. In practice, these observations will be extremely challenging as they require an exquisite stability of the telescope and the star over a period of days to tens of days. Future and more precise observatories, such as the Origins Space Telescope in the infrared or LUVOIR in the optical, will be more likely to obtain phase curve measurements of temperate planets.

Interpreting further the shape of these temperate rocky planet phase curves will be complex, as the number of unconstrained parameters that can influence the phase curve of a rocky planet is larger than the ones influencing a hot Jupiter, for which we already face many challenges. Among them are the large range of possible atmospheric composition ([Leconte et al. 2015a](#)), the possibility of asynchronous rotation ([Leconte et al. 2015b](#)), the range of possible atmospheric mass ([Koll and Abbot 2015](#)), the thermal inertia of the ground ([Selsis et al. 2013](#)), the peculiar behavior of clouds ([Yang et al. 2013](#)), the effects of non-dilute atmospheres ([Pierrehumbert and Ding 2016](#)) or the intertwined signal of different planets (including undetected ones) on the same system ([Kane and Gelino 2013](#)).

## Conclusion

Exoplanet phase curves are fundamental probes of the three-dimensional structure of exoplanets in close-in orbits. The current sample shows that every exoplanet studied so far is unique, making the search for trends between phase curve shape and

planetary parameters harder. State-of-the-art models are unable to quantitatively explain current phase curve observations. Whether clouds, drag, atmospheric variability, chemistry, or instrumental systematics are behind the unexpectedly large amplitude and small offsets of hot Jupiters, thermal phase curves should be determined in the near future through the wavelength dependence of the phase curve shape as will be observed by coming spacecrafts. Numerous observations of cooler and smaller planets are expected in the next decade and will probably challenge our current understanding of planetary atmospheres.

## Cross-References

- Observing Exoplanets with the Spitzer Space Telescope
- Characterization of Exoplanets: Secondary Eclipses
- Mapping Exoplanets
- Exoplanet Atmosphere Observations from Transmission Spectroscopy and Other Planet-Star Combined Light Observational Techniques
- Atmospheric Circulation for Exoplanet Atmospheres
- Radiative Transfer for Exoplanet Atmospheres

**Acknowledgements** We thanks Kevin Stevenson for useful feedback on the manuscript. V.P. acknowledges support from the Sagan Postdoctoral Fellowship through the NASA Exoplanet Science Institute.

## References

Agúndez M, Parmentier V, Venot O, Hersant F Selsis F (2014) Pseudo 2d chemical model of hot-jupiter atmospheres: application to hd 209458b and hd 189733b. *A&A* 564:A73, URL <http://dx.doi.org/10.1051/0004-6361/201322895>

Arcangeli J, Desert JM, Line M et al. (2017) Hst phase curve of the hot jupiter wasp-18b. in prep

Armstrong DJ, de Mooij E, Barstow J et al. (2016) Variability in the atmosphere of the hot giant planet hat-p-7 b. *Nature Astronomy* 1:0004 EP –, URL <http://dx.doi.org/10.1038/s41550-016-0004>

Batygin K, Stanley S Stevenson DJ (2013) Magnetically Controlled Circulation on Hot Extrasolar Planets. *ApJ*776:53

Cooper CS Showman AP (2006) Dynamics and Disequilibrium Carbon Chemistry in Hot Jupiter Atmospheres, with Application to HD 209458b. *ApJ*649:1048–1063

Cowan NB Agol (2011a) The Statistics of Albedo and Heat Recirculation on Hot Exoplanets. *ApJ*729:54

Cowan NB Agol E (2008) Inverting Phase Functions to Map Exoplanets. *ApJ*678:L129–L132

Cowan NB Agol E (2011b) A Model for Thermal Phase Variations of Circular and Eccentric Exoplanets. *ApJ*726:82

Cowan NB, Machalek P, Croll B et al. (2012) Thermal Phase Variations of WASP-12b: Defying Predictions. *ApJ*747:82

Crossfield IJM (2015) Observations of Exoplanet Atmospheres. *PASP*127:941–960

Crossfield IJM, Hansen BMS, Harrington J et al. (2010) A New 24  $\mu\text{m}$  Phase Curve for  $\nu$  Andromedae b. *ApJ*723:1436–1446

Crossfield IJM, Knutson H, Fortney J et al. (2012) Spitzer/MIPS 24  $\mu\text{m}$  Observations of HD 209458b: Three Eclipses, Two and a Half Transits, and a Phase Curve Corrupted by Instrumental Sensitivity Variations. *ApJ*752:81

de Wit J, Lewis NK, Langton J et al. (2016) Direct Measure of Radiative and Dynamical Properties of an Exoplanet Atmosphere. *ApJ*820:L33

Demory BO, de Wit J, Lewis N et al. (2013) Inference of Inhomogeneous Clouds in an Exoplanet Atmosphere. *ApJ*776:L25

Demory BO, Gillon M, de Wit J et al. (2016) A map of the large day-night temperature gradient of a super-Earth exoplanet. *Nature*532:207–209

Dyudina UA, Sackett PD, Bayliss DDR et al. (2005) Phase Light Curves for Extrasolar Jupiters and Saturns. *ApJ*618:973–986

Esteves LJ, De Mooij EJW Jayawardhana R (2015) Changing Phases of Alien Worlds: Probing Atmospheres of Kepler Planets with High-precision Photometry. *ApJ*804:150

Evans TM, Sing DK, Kataria T et al. (2017) An ultrahot gas-giant exoplanet with a stratosphere. *Nature*548:58–61

Feng YK, Line MR, Fortney JJ et al. (2016) The Impact of Non-uniform Thermal Structure on the Interpretation of Exoplanet Emission Spectra. *ApJ*829:52

Fortney JJ, Lodders K, Marley MS Freedman RS (2008) A Unified Theory for the Atmospheres of the Hot and Very Hot Jupiters: Two Classes of Irradiated Atmospheres. *ApJ*678:1419–1435

Fromang S, Leconte J Heng K (2016) Shear-driven instabilities and shocks in the atmospheres of hot Jupiters. *A&A*591:A144

Garcia Munoz A Isaak KG (2015) Probing exoplanet clouds with optical phase curves. *ArXiv e-prints*

Guillot T, Burrows A, Hubbard WB, Lunine JI Saumon D (1996) Giant Planets at Small Orbital Distances. *ApJ*459:L35

Harrington J, Hansen BM, Luszcz SH et al. (2006) The Phase-Dependent Infrared Brightness of the Extrasolar Planet  $\nu$  Andromedae b. *Science* 314:623–626

Haynes K, Mandell AM, Madhusudhan N, Deming D Knutson H (2015) Spectroscopic Evidence for a Temperature Inversion in the Dayside Atmosphere of Hot Jupiter WASP-33b. *ApJ*806:146

Heng K (2012) On the Existence of Shocks in Irradiated Exoplanetary Atmospheres. *ApJ*761:L1

Heng K Demory BO (2013) Understanding Trends Associated with Clouds in Irradiated Exoplanets. *ApJ*777:100

Hu R, Demory BO, Seager S, Lewis N Showman AP (2015) A Semi-analytical Model of Visible-wavelength Phase Curves of Exoplanets and Applications to Kepler- 7 b and Kepler- 10 b. *ApJ*802:51

Hubeny I, Burrows A Sudarsky D (2003) A Possible Bifurcation in Atmospheres of Strongly Irradiated Stars and Planets. *ApJ*594:1011–1018

Hut P (1981) Tidal evolution in close binary systems. *A&A*99:126–140

Iro N, Bézard B Guillot T (2005) A time-dependent radiative model of HD 209458b. *A&A*436:719–727

Kane SR Gelino DM (2013) Decoupling Phase Variations in Multi-planet Systems. *ApJ*762:129

Kataria T, Showman AP, Lewis NK et al. (2013) Three-dimensional Atmospheric Circulation of Hot Jupiters on Highly Eccentric Orbits. *ApJ*767:76

Kataria T, Showman AP, Fortney JJ et al. (2015) The Atmospheric Circulation of the Hot Jupiter WASP-43b: Comparing Three-dimensional Models to Spectrophotometric Data. *ApJ*801:86

Knutson HA, Charbonneau D, Allen LE et al. (2007) A map of the day-night contrast of the extrasolar planet HD 189733b. *Nature*447:183–186

Knutson HA, Charbonneau D, Cowan NB et al. (2009) Multiwavelength Constraints on the Day-Night Circulation Patterns of HD 189733b. *ApJ*690:822–836

Knutson HA, Lewis N, Fortney JJ et al. (2012) 3.6 and 4.5  $\mu\text{m}$  Phase Curves and Evidence for Non-equilibrium Chemistry in the Atmosphere of Extrasolar Planet HD 189733b. *ApJ*754:22

Koll DDB Abbot DS (2015) Deciphering Thermal Phase Curves of Dry, Tidally Locked Terrestrial Planets. *ApJ*802:21

Komacek TD Showman AP (2016) Atmospheric Circulation of Hot Jupiters: Dayside/Nightside Temperature Differences. *ApJ*821:16

Komacek TD, Showman AP Tan X (2017) Atmospheric Circulation of Hot Jupiters: Dayside/Nightside Temperature Differences. II. Comparison with Observations. *ApJ*835:198

Kreidberg L Loeb A (2016) Prospects for Characterizing the Atmosphere of Proxima Centauri b. *ApJ*832:L12

Kreidberg L, Parmentier V, Line M et al. (2017) Global Climate of the Ultra-Hot Jupiter WASP-103b from HST and Spitzer Phase Curve Observations. in prep

Krick JE, Ingalls J, Carey S et al. (2016) Spitzer IRAC Sparsely Sampled Phase Curve of the Exoplanet Wasp-14B. *ApJ*824:27

Langton J Laughlin G (2008) Hydrodynamic Simulations of Unevenly Irradiated Jovian Planets. *ApJ*674:1106-1116

Leconte J, Forget F Lammer H (2015a) On the (anticipated) diversity of terrestrial planet atmospheres. *Experimental Astronomy* 40:449–467

Leconte J, Wu H, Menou K Murray N (2015b) Asynchronous rotation of Earth-mass planets in the habitable zone of lower-mass stars. *Science* 347:632–635

Lee G, Dobbs-Dixon I, Helling C, Bognar K Woitke P (2016) Dynamic mineral clouds on HD 189733b. I. 3D RHD with kinetic, non-equilibrium cloud formation. *ArXiv e-prints*

Lewis NK, Knutson HA, Showman AP et al. (2013) Orbital Phase Variations of the Eccentric Giant Planet HAT-P-2b. *ApJ*766:95

Lewis NK, Parmentier V, Kataria T et al. (2017) Atmospheric Circulation and Cloud Evolution on the Highly Eccentric Extrasolar Planet HD 80606b. *ArXiv e-prints*

Line MR Parmentier V (2016) The Influence of Nonuniform Cloud Cover on Transit Transmission Spectra. *ApJ*820:78

Maxted PFL, Anderson DR, Doyle AP et al. (2013) Spitzer 3.6 and 4.5  $\mu$ m full-orbit light curves of WASP-18. *MNRAS*428:2645–2660

Millholland S Laughlin G (2017) Supervised Learning Detection of Sixty Non-Transiting Hot Jupiter Candidates. *ArXiv e-prints*

Oreshenko M, Heng K Demory BO (2016) Optical phase curves as diagnostics for aerosol composition in exoplanetary atmospheres. *MNRAS*457:3420–3429

Parmentier V, Showman AP Lian Y (2013) 3D mixing in hot Jupiters atmospheres. I. Application to the day/night cold trap in HD 209458b. *A&A*558:A91

Parmentier V, Guillot T, Fortney JJ Marley MS (2015) A non-grey analytical model for irradiated atmospheres. II. Analytical vs. numerical solutions. *A&A*574:A35

Parmentier V, Showman AP de Wit J (2015) Unveiling the atmospheres of giant exoplanets with an echo-class mission. *Experimental Astronomy* 40(2):481–500, URL <http://dx.doi.org/10.1007/s10686-014-9395-0>

Parmentier V, Fortney JJ, Showman AP, Morley C Marley MS (2016) Transitions in the Cloud Composition of Hot Jupiters. *ApJ*828:22

Parmentier V, Showman AP, Fortney J Marley M (2017) The cloudy shape of hot Jupiters phase curves. in prep

Perez-Becker D Showman AP (2013) Atmospheric Heat Redistribution on Hot Jupiters. *ApJ*776:134

Perna R, Menou K Rauscher E (2010) Magnetic Drag on Hot Jupiter Atmospheric Winds. *ApJ*719:1421–1426

Perna R, Heng K Pont F (2012) The Effects of Irradiation on Hot Jovian Atmospheres: Heat Redistribution and Energy Dissipation. *ApJ*751:59

Pierrehumbert RT Ding F (2016) Dynamics of atmospheres with a non-dilute condensable component. *Proceedings of the Royal Society of London Series A* 472:20160107

Piskorz D, Benneke B, Crockett NR et al. (2017) Detection of Water Vapor in the Thermal Spectrum of the Non-Transiting Hot Jupiter  $\upsilon$  Andromedae b. *ArXiv e-prints*

Rogers TM (2017) Constraints on the magnetic field strength of HAT-P-7 b and other hot giant exoplanets. *Nature Astronomy* 1:0131

Rogers TM Komacek TD (2014) Magnetic Effects in Hot Jupiter Atmospheres. *ApJ*794:132

Schwartz JC Cowan NB (2015) Balancing the energy budget of short-period giant planets: evidence for reflective clouds and optical absorbers. *MNRAS*449:4192–4203

Schwartz JC, Kashner Z, Jovmir D Cowan NB (2017) Phase Offsets and the Energy Budgets of Hot Jupiters. *ArXiv e-prints*

Selsis F, Maurin AS, Hersant F et al. (2013) The effect of rotation and tidal heating on the thermal lightcurves of super Mercuries. *A&A*555:A51

Showman AP Guillot T (2002) Atmospheric circulation and tides of “51 Pegasus b-like” planets. *A&A*385:166–180

Showman AP Polvani LM (2011) Equatorial Superrotation on Tidally Locked Exoplanets. *ApJ*738:71

Showman AP, Cooper CS, Fortney JJ Marley MS (2008) Atmospheric Circulation of Hot Jupiters: Three-dimensional Circulation Models of HD 209458b and HD 189733b with Simplified Forcing. *ApJ*682:559–576

Showman AP, Fortney JJ, Lian Y et al. (2009) Atmospheric Circulation of Hot Jupiters: Coupled Radiative-Dynamical General Circulation Model Simulations of HD 189733b and HD 209458b. *ApJ*699:564–584

Shporer A (2017) The Astrophysics of Visible-light Orbital Phase Curves in the Space Age. *PASP*129(7):072,001

Shporer A Hu R (2015) Studying Atmosphere-dominated Hot Jupiter Kepler Phase Curves: Evidence that Inhomogeneous Atmospheric Reflection Is Common. *AJ*150:112

Steinrueck M, Parmentier V, Showman AP, Fortney J Lupu R (2017) How disequilibrium chemistry affects the phase curve of hot jupiters. *in prep*

Stevenson KB, Harrington J, Nymeyer S et al. (2010) Possible thermochemical disequilibrium in the atmosphere of the exoplanet GJ 436b. *Nature*464:1161–1164

Stevenson KB, Harrington J, Lust NB et al. (2012) Two nearby Sub-Earth-sized Exoplanet Candidates in the GJ 436 System. *ApJ*755:9

Stevenson KB, Bean JL, Madhusudhan N Harrington J (2014a) Deciphering the Atmospheric Composition of WASP-12b: A Comprehensive Analysis of its Dayside Emission. *ArXiv e-prints*

Stevenson KB, Désert JM, Line MR et al. (2014b) Thermal structure of an exoplanet atmosphere from phase-resolved emission spectroscopy. *Science* 346:838–841

Stevenson KB, Line MR, Bean JL et al. (2017) Spitzer Phase Curve Constraints for WASP-43b at 3.6 and 4.5  $\mu$ m. *AJ*153:68

Tsai SM, Dobbs-Dixon I Gu PG (2014) Three-dimensional Structures of Equatorial Waves and the Resulting Super-rotation in the Atmosphere of a Tidally Locked Hot Jupiter. *ApJ*793:141

Visscher C Moses JI (2011) Quenching of Carbon Monoxide and Methane in the Atmospheres of Cool Brown Dwarfs and Hot Jupiters. *ApJ*738:72

Visscher C, Lodders K Fegley B Jr (2006) Atmospheric Chemistry in Giant Planets, Brown Dwarfs, and Low-Mass Dwarf Stars. II. Sulfur and Phosphorus. *ApJ*648:1181–1195

Webber MW, Lewis NK, Marley M et al. (2015) Effect of Longitude-dependent Cloud Coverage on Exoplanet Visible Wavelength Reflected-light Phase Curves. *ApJ*804:94

Wong I, Knutson HA, Lewis NK et al. (2015) 3.6 and 4.5  $\mu$ m Phase Curves of the Highly Irradiated Eccentric Hot Jupiter WASP-14b. *ApJ*811:122

Wong I, Knutson HA, Kataria T et al. (2016) 3.6 and 4.5  $\mu$ m Spitzer Phase Curves of the Highly Irradiated Hot Jupiters WASP-19b and HAT-P-7b. *ApJ*823:122

Yang J, Cowan NB Abbot DS (2013) Stabilizing Cloud Feedback Dramatically Expands the Habitable Zone of Tidally Locked Planets. *ApJ*771:L45

Zellem RT, Lewis NK, Knutson HA et al. (2014) The 4.5  $\mu$ m Full-orbit Phase Curve of the Hot Jupiter HD209458b. *ApJ*790:53

Zhang X Showman AP (2017) Effects of Bulk Composition on the Atmospheric Dynamics on Close-in Exoplanets. *ApJ*836:73